Fast and Accurate Electric Field Model for Optimizing the Insulation Design of Magnetic Devices

Author(s):
Korthauer, Bastian; Biela, Jürgen

Publication date:
2021

Permanent link:
https://doi.org/10.3929/ethz-b-000514776

Originally published in:
https://doi.org/10.1109/DMC51747.2021.9529943

Fast and Accurate Electric Field Model for Optimizing the Insulation Design of Magnetic Devices

Bastian Korthauer and Jürgen Biela
Laboratory for High Power Electronic Systems (HPE)
ETH Zurich, Switzerland
korthauer@hpe.ee.ethz.ch

***Abstract*—A bottleneck in optimization procedures of magnetic components is the calculation of the electric field strength (e.g. for an optimized insulation design) since this is based either on a slow numerical field simulation or on rough approximations. Hence, a fast and accurate method for the electric field calculation in the winding window is crucial for a fast optimization process. This paper presents a novel electric field calculation method that combines a variable potential function with a Schwarz-Christoffel (SC) mapping. This leads to accurate results, that match Finite Element Method (FEM) simulations as close as $5\ \%$. The proposed method is more than 200 times faster than FEM and robust against parameter changes.**

***Index Terms*—Insulation Design, Electric Field Calculation, Schwarz-Christoffel Transformation, Insulation Optimization**

I. Introduction

The optimization of power electronic converters has emerged to one of the major topics in power electronics design in recent years. In order to find an optimal converter design, several thousand possible designs have to be calculated [1]–[3]. For limiting the computational effort, fast and at the same time highly accurate analytical models are required.

A key element in many power electronic systems are magnetic devices, which significantly influence the system volume and efficiency. For designing and optimizing the magnetic components not only models for the core and winding losses are required but also for the insulation design, especially at higher operating voltages. In order to optimize the insulation distances between the windings and the core (e.g. d_y and d_x in Fig. 1), the method presented in [4] can be used. There, a cumulative mean value of the electric field is calculated along a critical field path. The result is then compared to breakdown data of the insulation material. All calculated mean values have to be below the partial discharge inception field strength from the breakdown data to obtain a valid design. This method leads to a more accurate design than just applying the maximum field strength [5]. However, such a comprehensive insulation design requires an accurate calculation of the electric field within the critical areas. As an accurate electric field calculation usually needs relatively slow FEM simulations, this becomes a bottleneck in the optimization routine. Therefore, converter optimization procedures often use rather rough approximations for the insulation modeling [2], [6]–[8], which could result in an oversized transformer design or, in worst case, in a breakdown. Especially for modular medium voltage transformer topologies, as given in [7], an accurate insulation design is crucial, since in such systems the secondary side often has to isolate a high (DC) offset voltage. A typical transformer geometry as used e.g. in [7] is depicted on the left side in Fig. 1. The figure shows one half of a foil-winding transformer based on an E-core. As the secondary winding is subject to a high offset voltage with respect to ground, a high potential on the winding surface results. This surface potential increases approximately linear from $\phi_{\mathrm{foil,off}}$ at z_6 to $\phi_{\mathrm{foil,max}}$ at z_5 (c.f. right side of Fig. 1) due to the increasing secondary winding voltage per turn. Therefore, the highest electric field is expected to occur in the red marked critical field area in Fig. 1.

To efficiently calculate the electric field in this area, a fast and at the same time accurate electric field calculation method is needed. The most common approaches for an analytical field calculation are the Charge Simulation Method (CSM) and the Conformal Map (CM) [5], [9]–[12]. The CSM is, however, not suitable for the investigated foil-winding transformer topology (c.f. Fig. 1), since many discrete simulation charges are required to accurately model the high surface charge density in the edges of the transformer winding [12], which results in long computation times. A more promising approach is a Conformal Map, which can be obtained by a Schwarz-Christoffel transformation. However, the downside of this method is that it assumes a constant potential along all boundaries. This leads to an inaccurate field approximation if applied to structures as given in Fig. 1, since the winding surface has a nonuniform potential. Therefore, a novel approach is presented in this paper, which extends the Schwarz-Christoffel Conformal Mapping by a redefined potential function. This enables an effective and accurate field calculation in critical areas of foil-winding transformers.

The structure of the paper is: First, the Schwarz-Christoffel

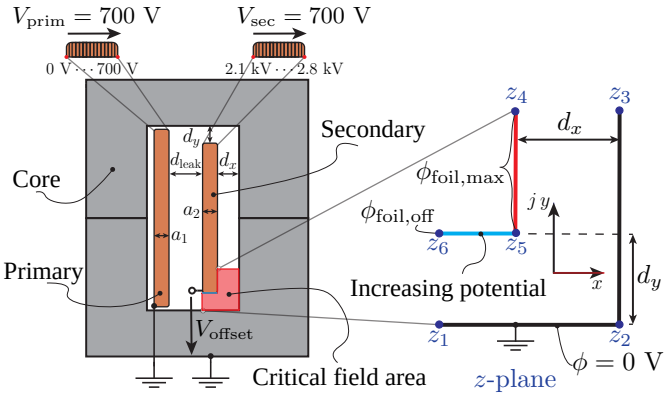

Fig. 1. Investigated transformer geometry, where the critical field area is highlighted (*left*) and the extracted polygon for the SC transformation in the z-plane (*right*).

transformation is explained briefly and a solution for the electric field in the critical area is derived. Next, the potential function in the image plane (w-plane) of the SC transformation is derived and a new electrical field solution is presented. Finally, the results of the basic and the improved approach are compared to FEM simulations within a comprehensive parameter study to investigate the overall accuracy and the influence of geometrical parameters.

II. Electric Field Calculation using SC Transformation

To obtain an analytical solution for the electric field in the critical field area in Fig. 1, a Conformal Map is derived. The Conformal Map provides an angle-preserving mapping of points in the z plane with $z = x + j\,y$, where the investigated polygon is transformed to an image plane with $\tau = \xi + j\,\eta$ using a mapping function $z = f(\tau)$ [11]. Since a conformal mapping function fulfils the two dimensional Laplace equation, it is suitable for electrostatic problems as well as problems regarding heat transfer or fluid flow [13].

A. Schwarz-Christoffel Transformation

To find a suitable conformal mapping function, the Schwarz-Christoffel transformation (1) can be used, which maps the interior of a polygon in the z-plane to the upper half of the τ-plane.

$$\frac{\partial z\,(\tau)}{\partial \tau} = \frac{C}{(\tau-\tau_1)^{\frac{\gamma_1}{\pi}} \cdot (\tau-\tau_2)^{\frac{\gamma_2}{\pi}} \cdot \ldots \cdot (\tau-\tau_N)^{\frac{\gamma_N}{\pi}}} \tag{1}$$

In (1), C is a complex constant, $\gamma_1, \ldots \gamma_N$ are the N exterior angles at the vertices $z_1, \ldots, z_N$ in the z-plane. These vertices map to the so called *prevertices* $\tau_1, \ldots, \tau_N$ in the τ-plane. By introducing a second SC transformation $\frac{\partial w}{\partial \tau}$ from a plane $w = u + j\,v$ to the same τ-plane, a transformation between two arbitrary geometries can be obtained by $\frac{\partial z}{\partial w} = \frac{\partial z}{\partial \tau} \cdot \frac{\partial \tau}{\partial w}$. If the geometry in the w-plane is chosen to represent an ideal plate capacitor, the v coordinate corresponds to the horizontally oriented equipotential lines. Hence, the transformation $\frac{\partial z}{\partial w}$ provides a mapping from the complex electric field in the z-plane to the simple field conditions of an ideal plate-capacitor in the w-plane. As the representation in the w-domain is the same for most electrostatic problems, solutions for the electric field in dependency of the transformation $\frac{\partial z}{\partial \tau}$ from the z-plane to the τ-plane can be found in literature [14]:

$$\begin{aligned} E_z(u,v) &= \left(j\,\frac{\partial w}{\partial z}\right)^* \\ &= \left(\frac{-j}{\pi}\,\frac{\phi_{\mathrm{foil,max}}}{\tau}\left(\frac{\partial z}{\partial \tau}\right)^{-1}\right)^*\Bigg|_{\tau=\exp(u+j\,v)} \end{aligned} \tag{2}$$

With the transformation $\frac{\partial z}{\partial \tau}$ from z-plane to τ-plane, a field calculation is possible.

B. Basic SC-Approach

For the investigated transformer topology, the critical field area (red area in Fig. 1) can be represented by the interior of the polygon depicted on the right side in Fig. 1. Hence, the SC transformation formula (1) results in:

$$\frac{\partial z}{\partial \tau} = C\,\sqrt{\frac{\tau-\mu}{\tau+1}}\,\frac{1}{\tau}, \tag{3}$$

By integrating (3) between known vertices in the z-plane, the unknown constants C and μ can be calculated.

$$C = -\frac{d_y}{\pi}, \qquad \mu = \left(\frac{d_x}{d_y}\right)^2 \tag{4}$$

Finally, an indefinite integration of (3) yields the mapping function from the w-plane to the z-plane.

$$z(w) = \frac{2\,d_x}{\pi}\arctan\left(\frac{\gamma}{d_x}\right) + \frac{d_y}{\pi}\ln\left(\frac{\gamma-d_y}{\gamma+d_y}\right) \tag{5}$$

$$\gamma = \sqrt{\frac{{d_y}^2\,\mathrm{e}^w - {d_x}^2}{\mathrm{e}^w+1}} \tag{6}$$

Since (2) describes the electric field in the z-plane in dependence of the spacial variables of the w-plane and (5) gives the transformation of the spacial variables from the w-plane to the z-plane, these two equations provide an analytic solution for the electric field in the investigated geometry. However, as already stated, the potential along the conductor is not constant but increases between the points z_6 and z_5 from $\phi_{\mathrm{foil,off}}$ to $\phi_{\mathrm{foil,max}}$ which is not considered in (2), since the potential at the underlying ideal plate capacitor has to be constant on both plates. As this can lead to an inaccurate field calculation an improved SC-approach, which takes a space-dependent potential into consideration, is presented in the following.

III. Improved SC-Approach

The principal idea of the proposed improved SC-approach is to replace the existing potential function in the w-plane by a new potential function $\phi(u,v)$. This potential function is chosen such, that it fulfils the specific boundary conditions (BCs) in the z-plane. In order to obtain the new potential function, it

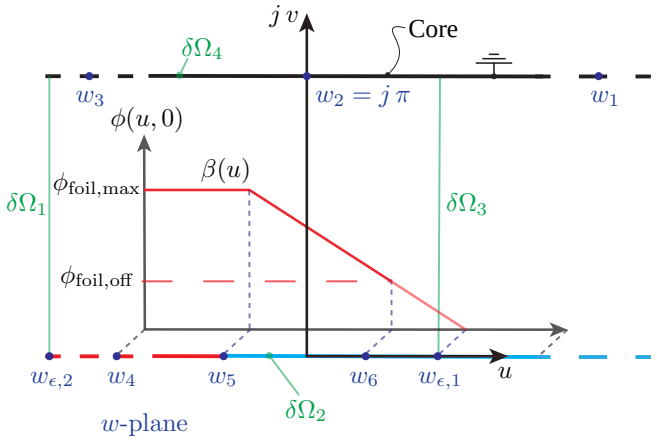

Fig. 2. Representation of transformer corner in the w-plane where it maps to two parallel electrodes.

is still useful to utilize the plate capacitor geometry in the w-plane as this simplifies the boundary value problem (BVP). Fig. 2 depicts the representation of the critical transformer corner (c.f. Fig. 1) in the w-plane. The four boundaries $\delta\Omega_1 - \delta\Omega_4$ for the BVP are depicted in green. Further, the blue points w_1 to w_6 are the images of the points z_1 to z_6 (c.f. Fig. 1). The points $w_{\epsilon,1}$ and $w_{\epsilon,2}$ are introduced additionally to describe the vertical boundaries $\delta\Omega_1$ and $\delta\Omega_3$. Using the mapping function (5), all images in the w-plane of the points in the z-plane can be calculated. This allows to map the BCs from the z-plane to the w-plane. The grounded walls of the core, map to a straight line in the w-plane at $v = \pi$. Therefore, the BC at $\delta\Omega_4$ yields $\phi(u,\pi) = 0$. The vertical boundaries $\delta\Omega_1$ and $\delta\Omega_3$ at $u = u_{\epsilon,1}$ and $u = u_{\epsilon,2}$, respectively, are set to zero. There, $u_{\epsilon,1}$ is shifted far away to obtain a constant potential at $u = u_4$ and $u_{\epsilon,2}$ is chosen such that $\phi(u_6, 0) = \phi_{\text{foil,off}}$. Accordingly, $u_{\epsilon,2}$ is:

$$u_{\epsilon,2} = \frac{\phi_{\text{foil,max}} \cdot u_6 - \phi_{\text{foil,off}} \cdot u_5}{\phi_{\text{foil,max}} - \phi_{\text{foil,off}}} \tag{7}$$

The boundary $\delta\Omega_2$ at $v = 0$ is the SC transformed surface of the winding. There, the potential is described by an arbitrary function $\beta(u)$. To represent the surface potential of the secondary winding, $\beta(u)$ is chosen as:

$$\beta(u) = \begin{cases} \phi_{\text{foil,max}} & \text{if } u \le u_5 \\ \frac{\phi_{\text{foil,max}} - \phi_{\text{foil,off}}}{u_5 - u_6}\, u + \frac{\phi_{\text{foil,max}} u_6 - \phi_{\text{foil,off}} u_5}{u_6 - u_5} & \text{if } u > u_5 \\ 0 & \text{if } u > u_{\epsilon,2} \end{cases} \tag{8}$$

Therefore, it describes a function, which has a constant potential $\phi_{\text{foil,max}}$ until $u = u_5$, from where it decreases linearly to $\beta(u = u_6) = \phi_{\text{foil,off}}$ (c.f. Fig. 2). Since u_5 is the transformed winding edge z_5, $\beta(u)$ describes the potential along the foil winding under the assumption of a linear increasing potential along the horizontal winding surface. As all boundary conditions are defined now, the new potential function $\phi(u,v)$ can be derived using a separation of variables approach and the application of "Fourier's trick" [15]:

$$\phi(u,v) = \sum_{m=1}^{\infty} \left(A_m \sin(k_u\, u') \sinh(k_u\, v')\right) \tag{9}$$

$$A_m = \frac{2}{u'_{\epsilon,2} \sinh(k_u\, \pi)} \int_0^{u'_{\epsilon,2}} \beta(u') \sin(k_u\, u')\, \mathrm{d}u' \tag{10}$$

where:

$$k_u = \frac{m\,\pi}{u'_{\epsilon,2}}, \qquad u' = u - u_{\epsilon,1}, \qquad v' = \pi - v$$
$$u'_5 = u_5 - u_{\epsilon,1}, \qquad u'_6 = u_6 - u_{\epsilon,1}. \tag{11}$$

There, $u'_{\epsilon,2}$ can be obtained from (7) if u_5 and u_6 are replaced by u'_5 and u'_6. Since (2) only applies for a constant electrode potential, a new electric field formula has to be derived. This can be done by calculating the gradient of the potential with respect to the z coordinates and exploiting the Cauchy–Riemann equations [11].

$$E_z(u,v) = -\mathrm{grad}_z\left(\phi(u,v)\right) \quad = \left(\frac{\partial \phi}{\partial w}\,\frac{\partial w}{\partial z}\right)^* \tag{12}$$

Hence, the electric field generated by the assumed potential function can be obtained from the derivative of the potential (9) and the derivative of the mapping function (5) with respect to w. Comparing (12) and (2), it can be seen that (2) is just a special case of (12) for $\phi(u,v) = v$.

The resulting plots for the electric potential and electric field are depicted in Fig. 3 and Fig. 4, respectively. To obtain the depicted figures, the summation in (9) is conducted for 30 coefficients. Fig. 3 also shows that the electric potential along the surface of the foil winding shows the same behaviour as defined in (8) (c.f. Fig. 2). The observable ringing of the surface potential function is a consequence of the limitation of the Fourier series in (9) to 30 coefficients. As this does not significantly affect the overall field solution using only 30 coefficients is usually sufficient. Due to the Fourier series a longer calculation time results compared to the basic approach. Thus, the next section presents a parameter study to determine how the chosen geometric parameters affect the overall accuracy of the electric field solution. This provides a guideline for choosing the most appropriate field calculation approach for a given parameter range.

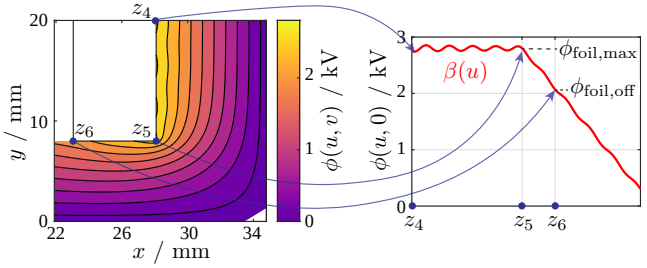

Fig. 3. Electric potential resulting from the improved SC-approach. The graph on the right side depicts the potential along the winding surface.

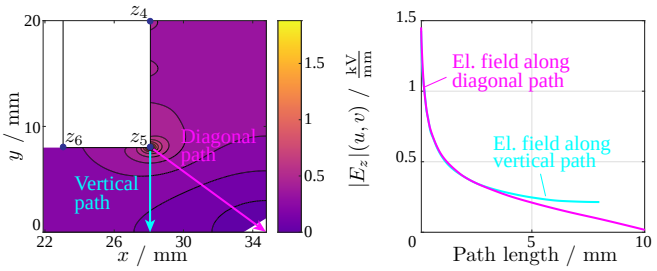

(a) Electric field resulting from the improved SC-approach.

(b) Electric field strengths along the vertical and diagonal field path.

Fig. 4. Calculated 2D and 1D electric field solutions using the improved SC-approach.

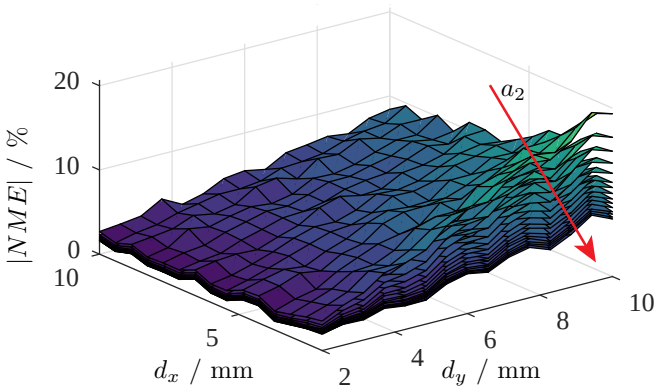

(a) *NME* in dependency of geometrical parameters – basic SC-approach.

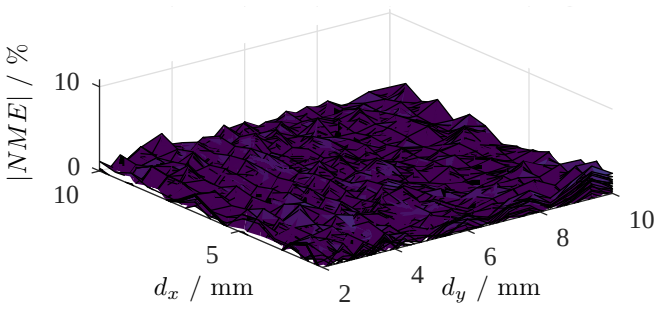

(b) *NME* in dependency of geometrical parameters – improved SC-approach.

Fig. 5. Comparison of the normalized mean error in dependency of geometrical parameters along the vertical path using the basic (a) and the improved SC-approach (b). For better comparison, the absolute value of the *NME* is shown.

IV. Parameter Study

The parameter study is performed for both approaches and validated using a 2D FEM simulation of the transformer geometry (c.f. Fig. 1). All used transformer specifications are chosen based on [7] (c.f. Fig. 1). However, the geometrical parameters secondary winding width a_2, insulation distance d_x and insulation distance d_y are swept in 15 steps between $2\,\mathrm{mm}$ and $10\,\mathrm{mm}$ yielding a total of 3375 simulations. The parameter ranges are chosen such that they enclose the respective parameters of the transformer design in [7]. The electric field obtained with the FEM simulations is then compared to the calculated electric field along the two paths shown in Fig. 4. These are two possible critical field paths, which can be used in the optimization procedure of the transformer insulation [4]. To speed up the FEM simulations, only the electric field along these paths is calculated. However, the simulation of all parameter-sets took, in average, more than 200 times longer than the same calculation using the improved SC-approach.

Since the insulation optimization procedure utilizes the mean value of the electric field along a critical path, the relative error of the calculated mean values is investigated to derive a proper figure of merit for comparison. The relative error between the mean value of the simulated and the calculated field can be expressed with

$$\delta_{\bar{E}_z} = \frac{\frac{1}{d}\int_0^d E_z(u,v)\,\mathrm{d}z - \frac{1}{d}\int_0^d E_{z,\mathrm{FEM}}(u,v)\,\mathrm{d}z}{\frac{1}{d}\int_0^d E_{z,\mathrm{FEM}}(u,v)\,\mathrm{d}z} = \frac{\frac{1}{d}\int_0^d E_z(u,v) - E_{z,\mathrm{FEM}}(u,v)\,\mathrm{d}z}{\frac{1}{d}\int_0^d E_{z,\mathrm{FEM}}(u,v)\,\mathrm{d}z} =: NME, \tag{13}$$

where d is the specific path length and $E_{z,\mathrm{FEM}}$ is the reference value resulting from the FEM simulation. It can be observed that (13) is equal to the mean error of E_z normalized by the mean value of the reference quantity. Hence, the normalized mean error (NME) of E_z will be taken as figure of merit for determining the accuracy of the proposed improved SC-approach in comparison to the basic SC-approach. Consequently, the accuracy of the electric field calculation along the critical field value can be expressed with only one quantity. For the error calculation, the field path is defined to start in a distance of $100\,\mu\mathrm{m}$ from the edge (c.f. z_5 in Fig. 1) to avoid the influence of the infinitely high edge field within the verification. Fig. 5 shows the results of the performed parameter study for the electric field comparison along the vertical path whereas Fig. 6 shows the results along the diagonal path. The results are presented as surface plots in dependency of the insulation distances d_y and d_x. For every simulated winding width a_2 one surface is generated. The plot in Fig. 5 (a) shows that by using the basic SC-approach for the electric field calculation, the NME can become higher than $20\ \%$. Furthermore, the error depends considerably on the geometrical parameters. Almost the same observation can be made for the error of the electrical field calculation along the diagonal path in Fig. 6 (a). With the improved SC-approach, however, no dependency of the investigated parameters can be observed for both cases. Moreover, the NME is for every set of parameters lower than the error of the basic SC-approach and is always smaller than $5\ \%$. To investigate to what extend the geometrical parameters influence the error of the basic SC-approach, a sensitivity analysis for each parameter is performed in the following section. In this analysis only the vertical path is investigated, since the error behaves similar for both critical field paths (c.f. Fig. 5 and Fig. 6).

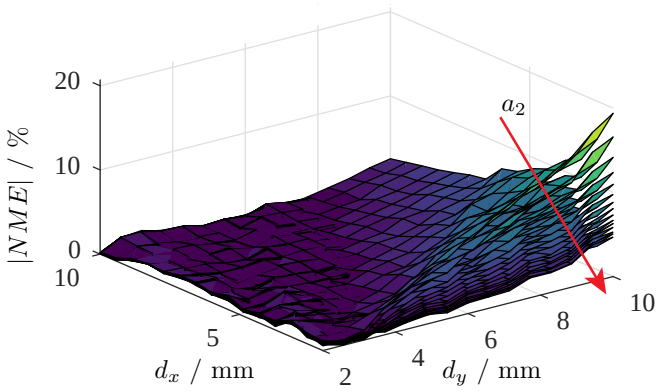

(a) *NME* in dependency of geometrical parameters – basic SC-approach.

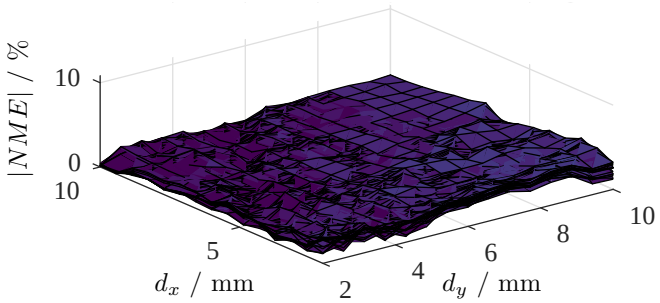

(b) *NME* in dependency of geometrical parameters – improved SC-approach.

Fig. 6. Comparison of the normalized mean error in dependency of geometrical parameters along the diagonal path using the basic (a) and the improved SC-approach (b). For better comparison, the absolute value of the *NME* is shown.

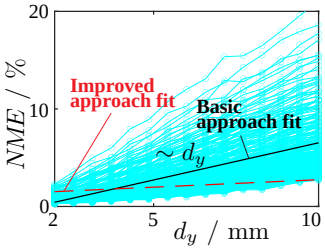

(a) *NME* dependency on d_y

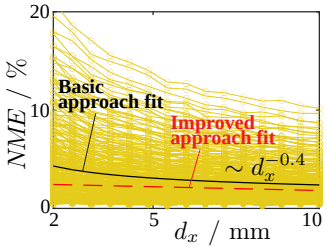

(b) *NME* dependency on d_x

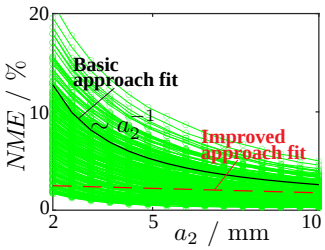

(c) *NME* dependency on a_2

Fig. 7. *NME* as function of different geometrical parameters. The colored curves depict the *NME*-dependency of the basic approach. The solid black lines represent the mean curve fit for the colored curves. The dashed red lines are the linear fit for the the improved SC-approach (Fit lines calculated from absolute error values).

A. Parameter Sensitivity Analysis

To examine how the different geometrical parameters affect the accuracy of the electrical field calculation, the influence on the normalized mean error is investigated for each parameter separately. The results in Fig. 7 (a), (b) and (c) show the normalized mean error for the basic SC-approach in dependency of the geometrical parameters d_y, d_x and a_2, respectively. There, the error of every parameter-set is depicted by a circle. The colored solid lines connect those circles where all parameters, despite the investigated one, are constant. Thus, they represent the dependency of the *NME* on a single parameter. The solid black line in each plot is the curve fit for the colored curves. As the results for the improved SC-approach do not show a clear functional dependency, the linear regression fit line is used for comparison. This linear fit of the improved SC-approach is represented by the dashed red line in the figures. The results show that the basic SC-approach exhibits a clear error dependency, especially on the parameters d_y and a_2. Furthermore, a slight dependency on d_x can be observed in Fig. 7 (b). According to Fig. 7 (a), the normalized mean error rises linearly with the insulation distance d_y. For the winding width a_2, the error shows an inverse proportionality (c.f. Fig. 7 (c)). Hence, small winding widths in combination with a large insulation distance d_y result in a large calculation error (c.f. Fig. 5 (a)). Using the improved approach, almost no error dependency can be observed for every parameter as can be seen from the dashed red lines in Fig. 7 (a) - (c). Thus, the error of the electric field calculation is not affected by the choice of the geometrical parameters, which makes the improved SC-approach well suitable for optimization routines. However, the improved approach employs a Fourier series and is, therefore, almost two times slower than the basic SC-approach. Consequently, for small insulation distances d_y and thick windings, the basic approach may be preferable, since the error for this choice of parameters is only slightly higher compared to the improved approach.

B. Overall Accuracy

In the previous considerations, the normalized mean error was used as figure of merit, which was motivated by the insulation design procedure. However, the proposed method is also suitable for a variety of other problems which are based on the Laplace equation. Hence, to give an insight on the overall accuracy of the method, Fig. 8 depicts the relative error of the electric field along the vertical field path for all investigated parameter sets. Here, the relative error is calculated with

$$\delta_{E_z} = \frac{E_z - E_{z,\mathrm{FEM}}}{E_{z,\mathrm{FEM}}}. \tag{14}$$

Thus, the plots in Fig. 8 show the percental deviation of the calculated electric field values to the simulated electric field values for each point along the path. Consequently, an

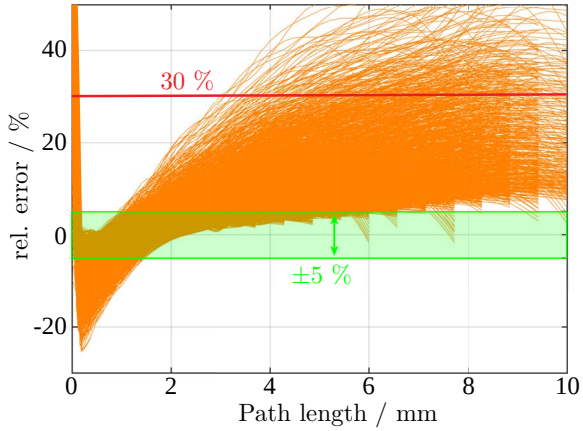

(a) Relative error vs. path length – basic SC-approach

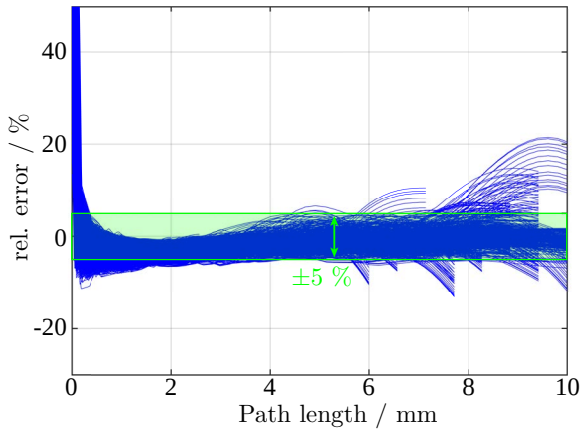

(b) Relative error vs. path length – improved SC-approach

Fig. 8. Relative errors of the electrical field calculations for all parameter-sets along the vertical critical field path with highlighted 5 % error range. The different lengths of the curves result from the different values for parameter d_y.

estimation for the spacial accuracy of the used calculation method is given. Fig. 8 (a) depicts the relative errors for the calculation with the basic approach, whereas Fig. 8 (b) depicts the errors of the improved approach. Despite a few outliers and a high error at very short path lengths caused by the infinitely high electric field in the winding edge, the relative calculation error of the improved approach lies mainly within a 5 % error range for almost the whole path length. The basic approach, however, exhibits a far higher relative error within a 30 % error range for most parameter-sets and can even become higher than 50 %. This emphasizes that also in terms of overall accuracy, the improved SC-approach is the more convincing field calculation method.

Conclusion

This paper presented a novel approach based on the SC transformation for an analytical calculation of the electric field in critical areas of foil winding transformers. The proposed method considers the varying potential along the conductor surface and, therefore, yields highly accurate results that match FEM simulations as close as 5 %. A comprehensive parameter study, which used the *NME* as figure of merit, revealed that the proposed method does not exhibit a significant dependency on geometrical parameters as it is the case for the basic SC-approach.

Due to the high accuracy, the robustness against parameter sweeps and the more than 200 times shorter calculation time compared to FEM, the proposed method is well suitable for electric field calculations in optimization routines. The proposed approach is also applicable to similar problems which are based on the Laplace equation and which exhibit an arbitrary potential along one boundary.

References

[1] M. Leibl, G. Ortiz, and J. W. Kolar, "Design and experimental analysis of a medium-frequency transformer for solid-state transformer applications," *IEEE Journal of Emerging and Selected Topics in Power Electronics*, vol. 5, no. 1, pp. 110–123, 2017.

[2] A. Fouineau, M. Guillet, B. Lefebvre, M. A. Raulet, and F. Sixdenier, "A medium frequency transformer design tool with methodologies adapted to various structures," in *15th Int. Conf. on Ecological Vehicles and Renewable Energies (EVER)*, 2020.

[3] A. Garcia-Bediaga, I. Villar, A. Rujas, L. Mir, and A. Rufer, "Multi-objective optimization of medium-frequency transformers for isolated soft-switching converters using a genetic algorithm," *IEEE Transactions on Power Electronics*, vol. 32, no. 4, pp. 2995–3006, 2017.

[4] F. Derler, H. Kirch, C. Krause, and E. Schneider, "Development of a design method for insulating structures exposed to electric stress in long oil gaps and along oil/transformerboard interfaces," in *7th Int. Symposium on High Voltage Engineering*.

[5] A. Küchler, *Hochspannungstechnik : Grundlagen - Technologie - Anwendungen*, 4th ed. Springer Berlin Heidelberg, 2017.

[6] M. Kharezy, M. Eslamian, and T. Thiringer, "Insulation design of a medium frequency power transformer for a cost-effective series high voltage dc collection network of an offshore wind farm," in *Proc. of the 21st Int. Symposium on High Voltage Engineering*, B. Németh, Ed. : , 2020, pp. 1406–1417.

[7] M. Stojadinović and J. Biela, "Modelling and design of a medium frequency transformer for high power dc-dc converters," in *Power Electronics Conference (IPEC-Niigata-ECCE Asia)*, 2018.

[8] M. A. Bahmani, T. Thiringer, and M. Kharezy, "Optimization and experimental validation of medium-frequency high power transformers in solid-state transformer applications," in *IEEE Applied Power Electronics Conference and Exposition (APEC)*, 2016.

[9] H. Singer, H. Steinbigler, and P. Weiss, "A charge simulation method for the calculation of high voltage fields," *IEEE Transactions on Power Apparatus and Systems*, vol. PAS-93, no. 5, pp. 1660–1668, 1974.

[10] S. V. Kulkarni, *Transformer engineering : design, technology, and diagnostics*, 2nd ed. Boca Raton, FL: Taylor & Francis, 2012.

[11] M. Beyer, *Hochspannungstechnik : Theoretische und praktische Grundlagen*, 1st ed. Springer Berlin Heidelberg, 1986.

[12] M. Beasley, "Comparative study of three methods for computing electric fields," *Proceedings of the Institution of Electrical Engineers*, vol. 126, pp. 126–134(8), January 1979.

[13] R. Schinzinger, *Conformal Mapping : Methods and Applications*. Amsterdam: Elsevier, 1991.

[14] E. Weber, "Die konforme Abbildung in der elektrischen Festigkeitslehre," *Archiv für Elektrotechnik*, vol. 17, pp. 174–200, 1926.

[15] D. J. Griffiths, *Introduction to Electrodynamics*, fourth edition. ed. Cambridge: Cambridge University Press, 2017.